WILEY-VCH

Spatiotemporal Delivery of pBMP2 and pVEGF by a Core-Sheath Structured Fiber-Hydrogel Gene-Activated Matrix Loaded with Peptide-Modified Nanoparticles for Critical-sized Bone Defect Repair

Shan He, Ju Fang, Chuanxin Zhong, Min Wang, and Fuzeng Ren**

Dr. S. He, Dr. J. Fang, C. X. Zhong, and Prof. F. Z. Ren

Department of Materials Science and Engineering, Southern University of Science and Technology, Shenzhen, Guangdong, China

Email: renfz@sustech.edu.cn

Dr. S. He and Prof. M. Wang

Department of Mechanical Engineering, The University of Hong Kong, Pokfulam Road, Hong Kong

Email: memwang@hku.hk

Keywords: gene-activated matrix, spatiotemporal, gene delivery, composite scaffold, bone regeneration

Abstract

The clinical translation of bioactive scaffolds for the treatment of large segmental bone defects remains a grand challenge. The gene-activated matrix (GAM) combining gene therapy and tissue engineering scaffold offers a promising strategy for the restoration of structure and function of damaged or dysfunctional tissues. Herein, we have developed a gene-activated biomimetic composite scaffold consisting of an electrospun poly(ε-caprolactone) (PCL) fiber sheath and an alginate hydrogel core which carried plasmid DNA encoding bone morphogenetic protein 2 (pBMP2) and vascular endothelial growth factor (pVEGF), respectively. A peptide-modified polymeric nanocarrier with low cytotoxicity and high efficiency serves as the non-viral DNA delivery vector. The obtained GAM allows spatiotemporal release of pVEGF and pBMP2 and promotes osteogenic differentiation of pre-osteoblasts *in vitro*. *In vivo* evaluation using a critical-sized segmental femoral defect model in rats shows that the dual gene delivery system can significantly accelerate bone healing by activating angiogenesis and osteogenesis. These findings demonstrate the effectiveness of the developed dual gene-activated core-sheath structured fiber-hydrogel composite scaffold for critical-sized bone defect regeneration and the potential of cell-free scaffold-based gene therapy for tissue engineering.

1. Introduction

Large bone defects resulted from trauma, infection and tumor resection represent a challenging clinical problem worldwide.[1] Due to the severely short supply of autografts, various tissue engineering strategies have been developed aiming to create artificial bone grafts to satisfy the pressing clinical need. Active participation of biomolecules greatly contributes to the progress of bone tissue engineering.[2] Especially, combinational use of vascular endothelial growth factor (VEGF), and bone morphologic protein 2 (BMP2) has been substantially employed for bone regeneration. BMP2 plays a central role in bone formation due to its high osteoinductive potential.[3] VEGF can not only promote angiogenesis but also drive the maturation of osteoblasts and cartilage osteogenesis, thereby accelerating bone regeneration.[4] The synergistic effect of VEGF and BMP2 in enhancing osteogenesis has been demonstrated in growth factor delivery-based studies.[2a, 5] However, their employment in gene delivery for vascularized bone regeneration is still in the early stage and require in-depth investigation.

Instead of a direct addition of growth factors, gene delivery-based strategy allows the production of BMP2 and VEGF by transfected cells via the manipulation of therapeutic genes, plasmid encoding BMP2 (pBMP2) and VEGF (pVEGF). Growth factors are normally delivered in high or repeated doses due to very short biological half-life, which not only increases the cost, but also possibly results in some unwanted side effects, such as heterotopic ossification, cancer risks, hypotension and edema.[6] By contrast, gene delivery can achieve long-term efficacy by allowing local protein expression through target cells at the defect site and extended protein production over time. Therapeutic genes can be incorporated in a three-dimensional scaffold to develop gene-activated matrix (GAM) for controlled gene delivery in clinical applications.[7] The GAM serves as a depot for genes and provides protection from extracellular barriers, including attack from the immune system and degradation by serum nuclease or proteases.[8] Moreover, the GAM allows localized gene delivery to cells with minimal off-target effects as host cells can be recruited to the bioactive scaffold.

As is known, tissue formation is a complicated cascade of events that involve a time-dependent expression of multiple signaling factors at specific locations, namely obeying a spatiotemporal pattern.[9] During the normal bone growth process, for instance, VEGF expression was exposed within the first week to induce angiogenesis while BMP2 acts within a duration of several weeks to promote osteogenic differentiation.[10] Thus, spatiotemporal delivery of multiple growth factors has been frequently investigated and demonstrated its benefit in promoting tissue regeneration.[10-11] Likewise, it is believed that spatiotemporal gene

delivery from biological scaffolds can orchestrate controlled protein expression to manipulate cell proliferation, differentiation, matrix synthesis, and final tissue repair.[12] Therefore, the design of GAMs should mimic the natural process as much as possible by obeying spatiotemporally controlled gene release to achieve efficient tissue regeneration. However, only a few examples exist for bioactive scaffolds enabling spatiotemporal delivery of multiple genes.[13]

In this study, we aim to develop a scaffold allowing spatiotemporal gene delivery of pBMP2 and pVEGF to promote vascularized bone regeneration. To achieve this, we combined a unique cylindrical core-sheath structured fiber-hydrogel scaffold and gene-carrying nanocomplexes to generate a bioactive GAM (**Figure 1)**. Specifically, the scaffold consisted of an electrospun poly(ε-caprolactone) (PCL) fiber sheath and an alginate hydrogel core, which incorporated pBMP2 and pVEGF, respectively. It is hypothesized that such a dual-gene delivery scaffold could be used as a bone grafting implant substitute, providing a conducive environment for new bone formation. The scaffold was systematically characterized to evaluate its physical properties, gene release behavior, and *in vitro* osteogenesis capability. The *in vivo* bone healing efficacy was evaluated using a critical-sized segmental femoral defect model in rats. Our findings provide deep insight into the design and fabrication of GAMs that are controllable, effective, and biocompatible, offering an effective therapeutic approach specifcally for bone tissue engineering.

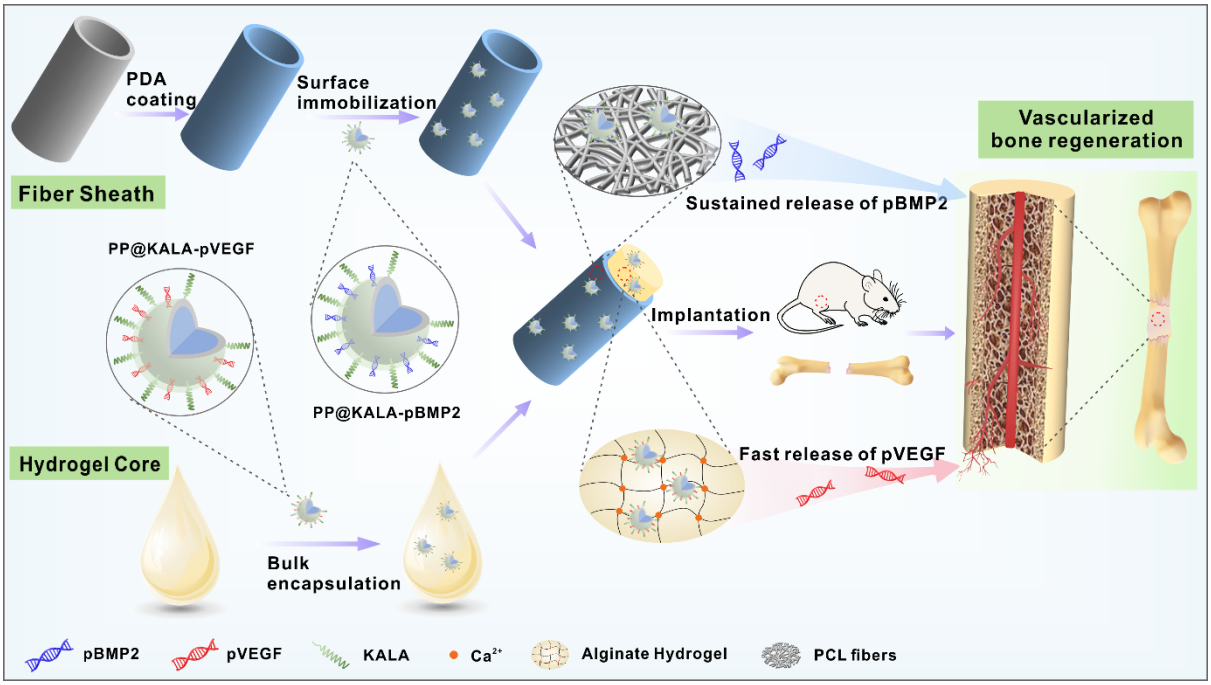

Figure 1. Schematic illustration of the core-sheath structured fiber-hydrogel composite scaffold carrying dual genes for critical-sized segmental bone defect repair. A PCL electrospun fiber sheath was firstly prepared and modified with a polydopamine coating before combining with the alginate hydrogel to form a composite scaffold. With well-defined incorporation of pBMP2 and pVEGF, the developed GAM system was able to manipulate spatiotemporal delivery of pVEGF and pBMP2 and to induce vascularized bone regeneration in a rat femoral defect model.

2. Results and discussion

2.1 Preparation and characterization of the core-sheath structured fiber-hydrogel GAM

Considering that tissue formation generally involves the time-dependent expression of multiple signaling factors at specific locations,[9a] it is of great significance to render a tissue engineering scaffold to allow spatiotemporal growth factor delivery to bring maximum tissue repairing effect.[9b, 10] As an alternative indirect strategy to growth factor delivery, it is also believed that gene delivery from scaffolds in a spatial and temporal manner can orchestrate controlled protein expression to manipulate cell proliferation, differentiation, matrix synthesis, and final tissue repair. In our study, spatiotemporal gene delivery was achieved within a fiber-hydrogel scaffold with a unique core-sheath structure (Figure 1). Specifically, the scaffold consisted of an electrospun PCL fiber sheath and an alginate hydrogel core. A polymeric non-viral vector with high transfection efficiency and low cytotoxicity, poly (D, L-lactic-co-glycolic acid)/polyethylenimine (PLGA/PEI) modified with the cell-penetrating peptide KALA (PP@KALA), which was developed previously in our group,[14] was used as the gene carrier. To achieve spatiotemporal gene delivery within the fiber-hydrogel composite scaffold, the PP@KALA nanocomplexes carrying pVEGF (PP@KALA-pVEGF) were physically encapsulated in the alginate hydrogel core, which can induce the fast release of pVEGF, while PP@KALA nanocomplexes carrying pBMP2 (PP@KALA-pBMP2) were immobilized to the electrospun polydopamine (PDA)-coated PCL fiber sheath, which can allow a slower release of pBMP2. With combined advantages, fiber-hydrogel composite scaffolds have gained their popularity in biomedical applications, particularly in drug delivery, which were commonly fabricated through a layer-by-layer stack of fiber mats and hydrogel layers or incorporation of small fragments of fiber mats into hydrogel.[15] However, to our knowledge, the present study is the first report in developing a cylindrical fiber-hydrogel composite scaffold for pDNA delivery.

Figure 2A showed the morphology of the electrospun PCL fiber sheath with Φ = 3 mm. The inset cross-sectional image indicated that the thickness of the fibrous wall was approximately 200-300 μm. After treated with NaOH, the water contact angle of the PCL fibers significantly decreased from 133.9º to 81.6º (Supplementary Figure S1), implying enhanced hydrophilicity. A functional PDA coating layer was attached to the fiber surface followed by the immobilization of PP@KALA-pBMP2 nanoparticles. Figure 2B demonstrated that a large number of nanoparticles were successfully immobilized and uniformly distributed on the surface of PDA-coated PCL fibers. When the fiber sheath was integrated with the hydrogel core

to form a composite scaffold (Supplementary Figure S2), a seamless interface between the hydrogel and the fibers after freeze-drying was observed (Figure 2C), which indicated that these two components with different nature could be combined into one integrated scaffold. The cross-sectional microscopic image at the fiber-hydrogel interface was shown in Figure 2D. It is observed that the hydrogels partially infiltrated into the fiber network, resulting in a continuous, integrated transition zone. Due to the dehydration process during sample preparation, the PCL fibers were wrapped by the collapsed hydrogel, forming a core-sheath fiber architecture with the increased fiber diameter (Figure 2D). Although this unique fiber architecture only appeared after freeze-drying, the results demonstrated that the hydrogel was mechanically interlocked by the porous and hydrophilic fiber network, suggesting successful fabrication of the core-sheath structured fiber-hydrogel composite scaffold. Regarding mechanical strength of the composite scaffold, it is the fiber sheath that made main contribution to a compressive strength of ~ 80 kPa while the hydrogel core could prevent the scaffold from large deformation or even collapse under stress (Supplementary Figure S5). With the incorporation of plasmids, the fluorescent image demonstrated the distribution of the plasmids both in the fiber sheath and hydrogel core of the 3D GAM (Supplementary Figure 2).

The fiber-hydrogel GAM, which carried pVEGF in the hydrogel core and pBMP2 on the PDA-coated fiber sheath, was expected to result in sequential gene delivery. Figure 2E showed the gene release profile of pBMP2 and pVEGF. The release of pVEGF showed an evident initial burst within 3 days and reached a plateau around day 7, showing that physical encapsulation of pVEGF in the hydrogel core led to very fast release due to fast diffusion of the DNA molecules and disintegration of alginate hydrogel. By contrast, pBMP2 was released at a slower rate without an obvious initial burst release. In fact, pBMP2 was released in a nearly zero-order manner in the first 96 hours (inset of Figure 2E). A sustained release of pBMP2 from the PDA-coated fibers for more than 21 days was observed before reaching a final plateau phase. It is presumed that there could be electrostatic interactions between negatively charged PDA and positively charged nanocomplexes,[16] as well as Michael addition reaction between o-quinones of PDA and amine and/or thiol groups of PEI and KALA in the nanocomplexes.[17] The resulted sequential gene release was expected to lead to a sequential protein production of VEGF and BMP2 in target cells, which is consistent with the temporal pattern of protein expression in natural bone formation.[18]

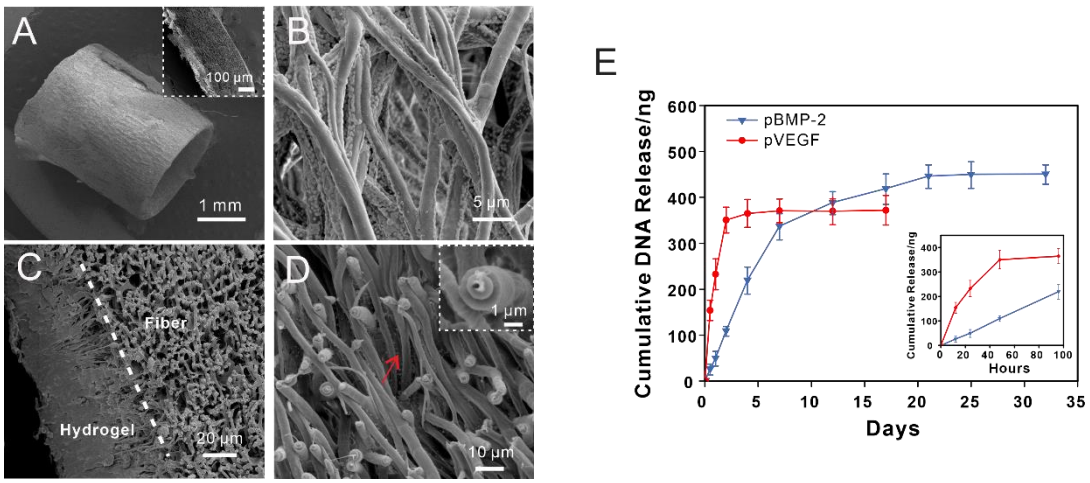

Figure 2. Characterization of the core-sheath structured fiber-hydrogel scaffold enabling spatiotemporal gene delivery. (A)–(D) are the SEM images of a PCL electrospun fiber sheath, PDA-coated fibers carrying PP@KALA-pBMP2 nanoparticles, the cross-section of fiber-hydrogel composite scaffold, and the cross section of PCL fibers with an inset of a single fiber in the composite scaffold, respectively. (E) The release kinetics of pBMP2 (blue triangles) and pVEGF (red circles) incorporated in the composite scaffold.

2.2 Transfection efficiency and cytotoxicity of PP@KALA

When it comes to gene delivery, an efficient delivery vehicle with minimal cytotoxicity is a primary requirement. In addition to various excellent cationic polymers, inlcuding poly (β-amino esters) (PBAEs),[19] poly (amidoamine) (PAMAM),[20] and chitosan,[21] composites/hybrids of different materials, for instance, peptide-modified polymeric carriers, have shown their potential due to combined advantages and all-sided performance in gene therapy.

In this study, we used a peptide-modified polymeric non-viral vector, PP@KALA, previously developed by our group,[14] which has an average particle size of ~ 200 nm, uniform morphology, and good biocompatibility and biodegradability. To evaluate the transfection efficiency of PP@KALA to treat MC3T3-E1 pre-osteoblasts, luciferase expression levels were quantitatively determined (**Figure 3**A). Similar levels of luciferase expression were observed in PP@KALA and PEI groups in the first two days. Peak levels were achieved at day 3 for both groups, but PP@KALA exhibited a slightly higher level. At day 5, the luciferase expression in PP@KALA group showed ~ 2.5 times higher than that of PEI group. Consistently, flow cytometery analysis (Supplementary Figure S4) demonstrated higher efficiency of PP@KALA than PEI, which is generally considered as a gold standard of transfection agent yielding high transfection efficiency in most cell lines,[22] suggesting the enhanced transfection efficiency and

more sustainable transfection capacity of PP@KALA. Notably, the transfection was carried out in serum-containing media. Many commercial gene vectors (e.g., liposomes) have higher efficiency in serum-free media, which cannot be replicated *in vivo*.[23] As PP@KALA showed excellent serum stability, the translational potential of this vector is more compelling.

The cytotoxicity of PP@KALA was investigated by CCK-8 assay. The results in Figure 3B suggested cells in all groups had a steady proliferation. However, the viability of PEI-transfected cells decreased at day 5 compared to the untransfected cells (blank), while PP@KALA group exhibited even higher cell viability than the blank, demonstrating the superior biocompatibility of PP@KALA. It is probably due to the favorable effect of KALA peptide, which has exhibited the capability to enhance cell proliferation.[24] In the results of GFP expression (Figure 3C), it was found that the two gene carriers showed obviously different effect on the morphology and intracellular fluorescence distribution of transfected MC3T3-E1s. GFP-positive cells in PP@KALA group showed elongated and well-spread morphology, whereas the PEI-transfected cells were in round or even abnormal shapes and many sand-like GFP spots were observed. Previous reports have demonstrated that PEI-associated cytotoxicity might derive from plasma-membrane destabilization and cellular organelles damage, which would then cause cell shrinkage, inhibited mitosis and vacuolization of the cytoplasm.[25]

For further observation of cell morphology, immunofluorescence staining was performed. Figure 3D revealed that MC3T3-E1 cells treated by PP@KALA exhibited a typical spindle or polygonal morphology with well-developed F-actin stress fibers and intensely stained focal adhesions. Instead, PEI-treated cells appeared much smaller with minimal spreading morphology and less organized F-actin fibers and focal adhesions. Semi-quantitative analysis of cell morphology revealed that the average surface area of cells transfected by PP@KALA was approximately 7-fold larger than that of PEI-treated cells and the average cell aspect ratio was 2-fold higher at day 1 and day 3 post-transfection (Figure 3E-F). It was possibly because the positively charged surface of PP@KALA nanocomplexes could enhance actin polymerization [26] and KALA peptide, a cell-penetrating peptide, has a major impact on membrane fluidity and internalization.[24b, 27] The first contacts between the cell-penetrating peptide and the cell surface take place through electrostatic binding with cell surface proteoglycans GlucosAminoGlycan (GAG) platform, followed by actin remodeling and a selective activation of Rho GTPases, which comprise a family of molecular switches that control signaling pathways.[28] Thereafter, the 'onset' of internalization of peptide carriers was triggered.[27b] The immunostaining results are consistent with the cytotoxicity study and GFP

expression analysis, demonstrating that PP@KALA with outstanding cell compatibility and enhanced transfection efficiency could be a superior gene carrier for osteoblasts.

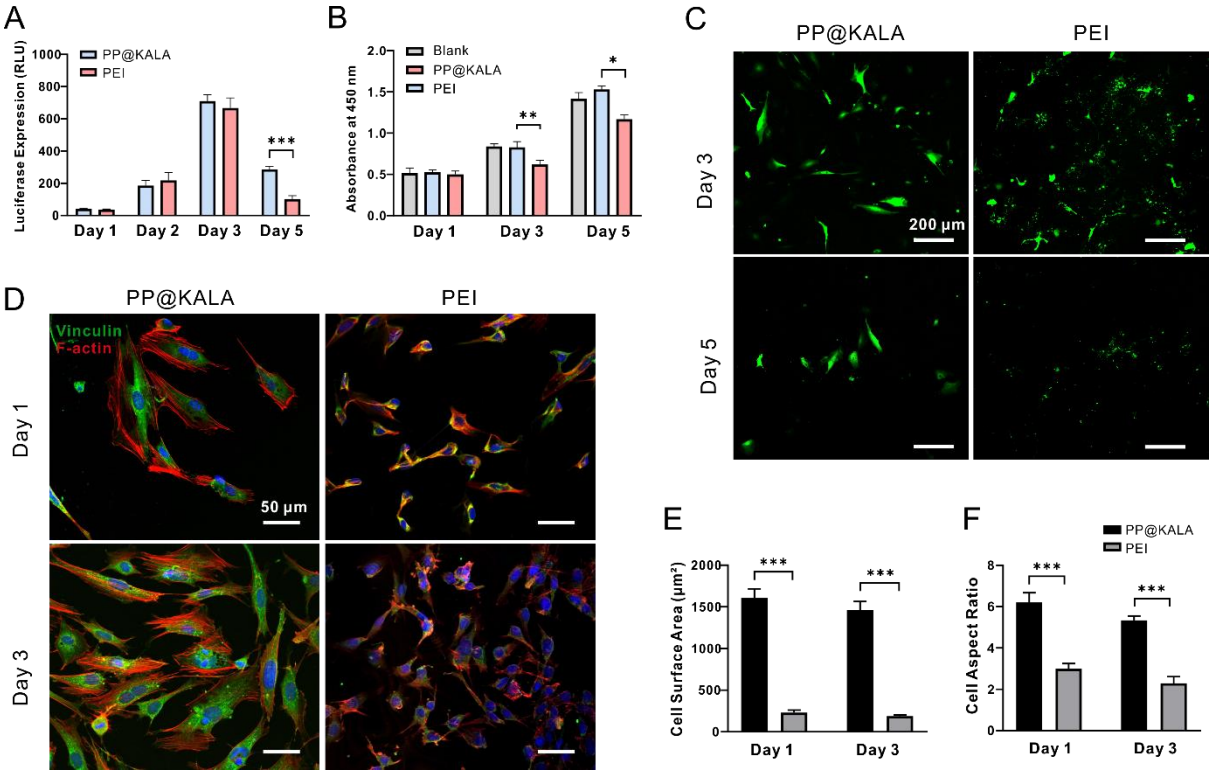

Figure 3. Transfection of MC3T3-E1 cells with PP@KALA nanocomplexes. (A) Luciferase expression. (B) Cell viability and proliferation. (C) GFP expression. (D) Immunofluorescent staining for vinculin (green), F-actin (red), nuclei (blue) at day 1 and day 3 post-transfection. (E) Cell surface area and (F) cell aspect ratio of the transfected cells measured based on images of (D). The data were plotted with mean ± standard deviation (n = 50). *$p < 0.05$, **$p < 0.01$, and ***$p < 0.001$.

2.3 Therapeutic gene delivery of pBMP2 and pVEGF by PP@KALA

To stimulate osteogenic potential, MC3T3-E1 cells were transfected by PP@KALA nanocomplexes carrying pBMP2 and pVEGF either individually or in combination (PP@KALA-pDual). The results (Figure 4A-B) showed that BMP2 and VEGF were secreted from transfected MC3T3-E1 cells for a sustained period of more than 7 days in both PP@KALA and PEI groups. Higher protein levels at day 3 than that at day 7 post-transfection indicated that PP@KALA-induced transfection led to fast transcription and translation. Encouragingly, higher levels of protein expression were produced by PP@KALA-treated cells than PEI-treated cells, demonstrating that PP@KALA-induced transfection could give rise to the effective production of target proteins.

To evaluate the functionality of BMP2 and VEGF produced by transfected cells in promoting osteogenic differentiation, the alkaline phosphatase (ALP) activity and gene expression of osteogenesis-related markers were characterized. Figure 4C revealed that all groups showed increased ALP activity from day 7 to day 14. Cells transfected by PP@KALA exhibited higher ALP levels than PEI-treated cells in the case of single gene delivery. For dual-gene delivery, no significant differences were shown between PP@KALA and PEI groups. In addition, it was observed that delivering pBMP2 led to the highest levels of ALP activity, possibly indicating that transgene expression of BMP2 was a major contributor to enhanced ALP activity of transfected MC3T3-E1 cells.

Gene expression levels of three osteogenic markers in transfected cells, including runt-related transcription factor 2 (Runx2), osteocalcin (OCN), and osteopontin (OPN), were assessed by real-time quantitative reverse transcription-polymerase chain reaction (RT-qPCR) (Figure 4D). At day 14, expression levels of all three markers in PP@KALA-treated cells, particularly Runx2 and OCN genes, were significantly up-regulated compared with PEI-treated cells. It is noted that the combinational delivery of pBMP2 and pVEGF did not exhibit superiority over single delivery of pBMP2. The main reason might be associated with the difference in pBMP2 dosage used in transfection, which can affect the protein production profiles and related signaling pathways. For pDual group, only a half dose of pBMP2 was delivered relative to single gene transfection, to keep a constant total pDNA dosage. As a key regulator in osteogenesis, BMP2 induced osteogenic differentiation effectively and directly. For another, some studies have demonstrated that synergistic effect of BMP2 and VEGF is not always at work unless with appropriate BMP2/VEGF ratios.[29] In addition, the outcome can be different when pBMP2 and pVEGF are sequentially delivered rather than simultaneously delivered into the target cells. Nevertheless, the results identified the potential of PP@KALA for therapeutic delivery of pBMP2 and pVEGF to osteoblasts in a highly efficient and safe manner to promote osteogenesis *in vitro*.

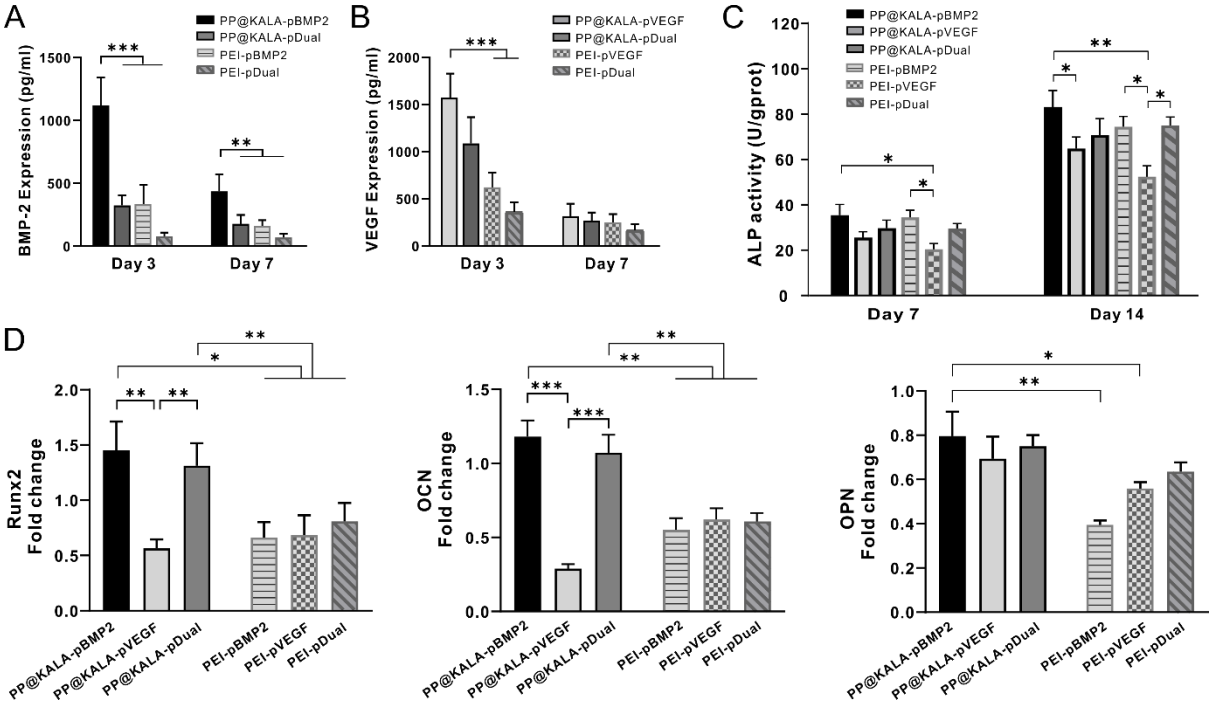

Figure 4. Therapeutic gene delivery of pBMP2 and pVEGF by PP@KALA nanocomplexes. (A) BMP2 and (B) VEGF protein expression of the transfected cells at day 3 and day 7 post-transfection. (C) ALP activity at day 7 and day 14 post-transfection. (D) mRNA expression of representative osteogenic genes, Runx2, OCN, and OPN, expressed by the transfected cells at day 14 post-transfection. The data were plotted with mean ± standard deviation ($n = 3$). *$p < 0.05$, **$p < 0.01$, and ***$p < 0.001$.

2.4 *In vitro* evaluation of the dual gene-activated matrix to promote osteogenic differentiation

To assess if the GAMs were capable to promote osteogenesis *in vitro*, calcium deposition and osteogenic gene expression were characterized. Calcium deposition is an indicator of osteogenic differentiation in the later stage, which could be visualized by alizarin red S staining. Four groups of scaffolds were prepared in this study: gene-free PCL/alginate scaffolds (P/A), PCL/alginate scaffolds with the core carrying pVEGF (P/A-pVEGF), PCL/alginate scaffolds with the sheath carrying pBMP2 (P/A-pBMP2), and PCL/alginate scaffolds carrying dual genes of pVEGF and pBMP2 (P/A-pDual).

The optical images of the stained scaffolds (Figure 5A) and related semi-quantitative analysis (Figure 5B) revealed that the MC3T3-E1 cells cultured on the gene-activated scaffolds produced more calcium nodules than those on gene-free scaffolds. Especially, P/A-pDual induced the highest level of calcium deposition. Interestingly, P/A-pVEGF showed a higher

level of calcium deposition than the P/A-pBMP2, possibly suggesting that VEGF signaling plays an essential role in promoting the maturation and mineral production of osteoblasts.[30]

Osteogenic differentiation was further evaluated by the mRNA expression of specific osteogenic markers and the angiogenic marker (Figure 5C). At day 7, significantly upregulated levels of ALP and VEGF in P/A-pDual group were observed, demonstrating the effect of dual gene delivery to stimulate early osteogenic differentiation and angiogenesis. Overall, increased gene expression levels were detected at day 14. A significant increase in Runx2 expression was observed in P/A-pBMP2 and P/A-pDual group, indicating that the incorporation of pBMP2 could be a major contributor to enhanced gene expression of Runx2, which is the earliest transcriptional regulator responsible for bone formation. Concerning the VEGF gene expression, obviously up-regulated levels were obtained in P/A-pVEGF group (~ 6 fold) and P/A-pDual group (~ 3.5 fold) at day 14. It should be noted that VEGF mRNA expression in this assessment can be derived from exogenous transgene expression induced by the GAM as well as endogenous secretion from osteoblasts. Collectively, the results of the expression profiles of all six genes at day 7 and day 14 indicated that P/A-pDual had a superior capacity to stimulate osteogenic differentiation of MC3T3-E1 cells *in vitro*. Interestingly, dual gene delivery exhibited its advantages over single delivery in P/A scaffold-based 3D system rather than PP@KALA-based 2D system, which can be attributed to the spatiotemporal release pattern and larger surface area for cell growth provided by the scaffold. More specifically, pVEGF and pBMP2 were simultaneously delivered into osteoblasts when cells were treated by PP@KALA nanocomplexes, whereas they were sequentially delivered into cells cultured in P/A-pDual scaffold, resulting in a protein expression manner in accordance with the native bone growth process. In addition, compared with the very limited surface in 2D monolayer culture, the 3D scaffold provided much a larger surface area for cell growth, which gave rise to prolonged transgene expression and thus better osteogenesis capability.

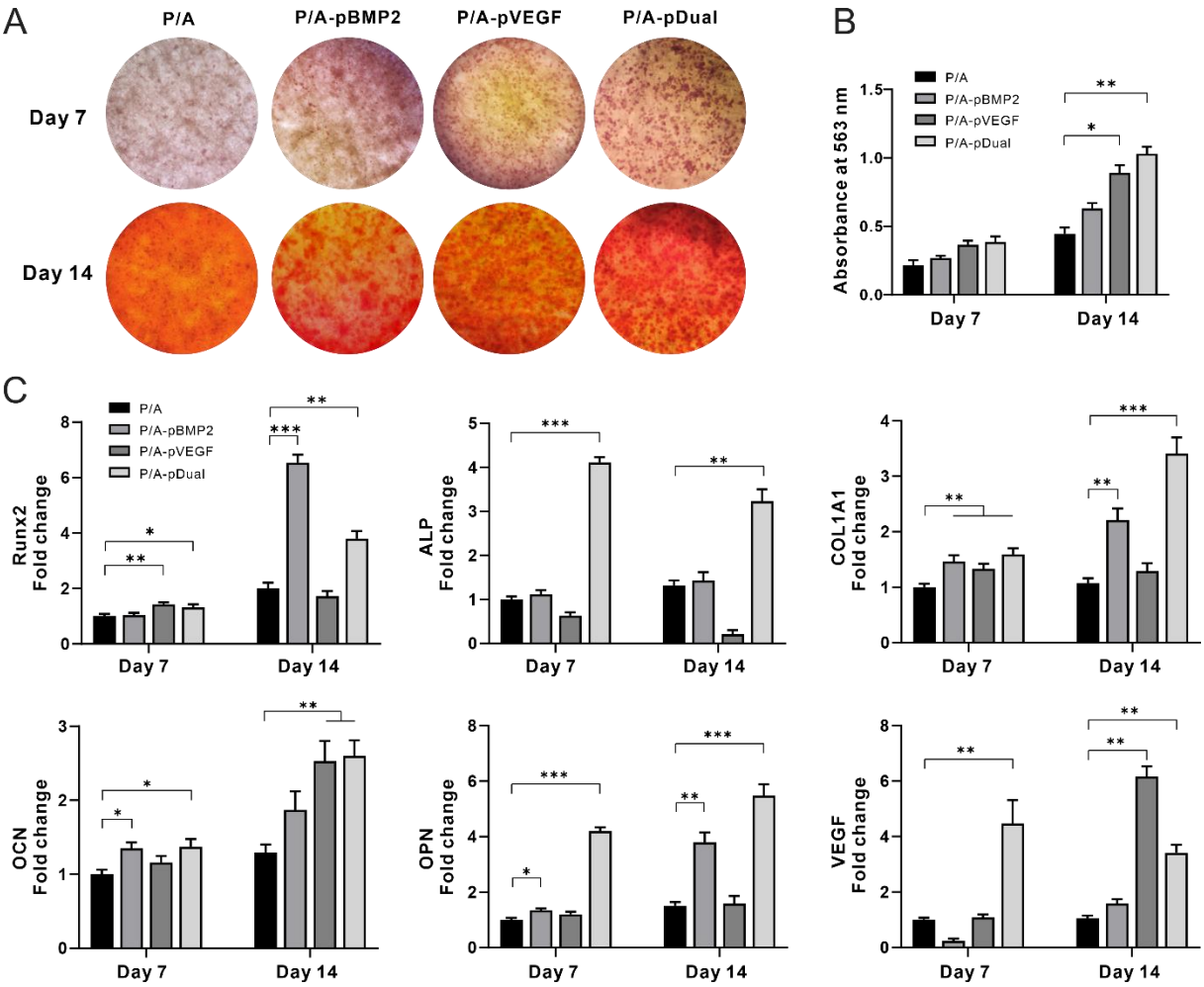

Figure 5. *In vitro* osteogenesis capability of the dual gene-activated scaffold. (A) Alizarin red staining for assessing calcium deposition on P/A, P/A-pBMP2, P/A-pVEGF and P/A-pDual scaffolds at day 7. (B) Semi-quantitative analysis for calcium deposition. (C) mRNA expression of ALP, Runx2, COL1, OCN, OPN and VEGF markers in cells cultured on various scaffolds. The data were plotted with mean ± standard deviation (n = 3). *$p < 0.05$, **$p < 0.01$, and ***$p < 0.001$.

2.5 *In vivo* evaluation of the dual gene-activated scaffold to accelerate critical-sized bone regeneration

Due to the great capacity of manipulating spatiotemporal release of pVEGF and pBMP, and the effectiveness to stimulate target genes expression *in vitro*, P/A-pDual was taken forward for *in vivo* implantation. The assessment of *in vivo* transgene expression was performed (Supplementary Figure S6). It is found that a large number of endogenous cells readily either adhere to or infiltrate throughout the implanted scaffold. The PP@KALA nanocomplexes carrying cy5-tagged pDNA are observed within the scaffold, revealing that the scaffold is

retaining the plasmid at the defect site. The presence of GFP positive cells demonstrates that host cells can be transfected *in vivo*.

Thereafter, the gene-delivering scaffold's potential of clinical translation was evaluated in a segmental femoral defect rat model (Figure 6A). It is a challenging model due to the large defect volume and the poor self-healing capacity, but provides persuasive findings for *in vivo* evaluation of bone repair.[31] Blank group (defect models without scaffold implantation) and P/A group (gene-free scaffolds) were used as control for comparison. After 8 weeks of implantation, the specimens were analyzed using μCT. Representative images of 3D reconstruction and 2D sagittal-view cross-sections (Figure 6B) clearly showed that minimal bone repair was observed in the blank defect which had a critical size of 5 mm, while in P/A group, a small amount of new bone was formed. By contrast, manifest bone healing was observed in the P/A-pDual group. Particularly, the defect was successfully bridged at cortical bone layer. The quantitative analysis of BV/TV showed that there was no significant difference between the blank and P/A group. However, the implantation of P/A-pDual led to a significantly higher level of new bone volume than the other two groups (~ 7-fold higher than blank, ~ 4-fold higher than P/A, $***p < 0.001$) (Figure 6C). The results of BMD analysis further confirmed the capacity of P/A-pDual for accelerated new bone formation, which agrees with the BV/TV data.

Histological analysis by Hematoxylin and eosin (H&E) staining was performed to assess bone regeneration. Representative images captured at the end and the central region of defect sites were shown in Figure 7. After 4 weeks, newly formed bone along the defect end was observed in scaffold-implanted groups. In P/A group, new bone tissue was only formed at the peripheral region of native bone fracture. The central area of defect was mainly filled with fibrous tissue, showing the limited capacity of gene-free scaffolds to induce new bone formation. In P/A-pDual group, a larger amount of newly formed woven bone was observed both at the end and central region. The light pink color suggested the immaturity of regenerated bone at defect site. Encouragingly, many blood vessels surrounding the new bone were observed in P/A-pDual group, which could probably further promote bone remodeling. After 8 weeks, good continuity between the newly formed bone and host bone was achieved in P/A group and P/A-pDual group. Especially, P/A-pDual group displayed better osteointegration at the defect end and allowed reconstitution of marrow cavity around the bridged bone. Nevertheless, the higher magnification images in the central region of defect clearly revealed different bone regeneration outcomes in scaffold-implanted groups. Only a small number of in-situ formed bone islands,

which were immature and unmineralized (light pink), were populated with fibrous tissue in P/A group. P/A-pDual group demonstrated a significantly larger amount of lamellar bone, which was mature and mineralized (dark pink). On the contrary, defect remained unhealed in the blank group, but was only filled with fibrous tissue and sporadically distributed bone islands.

Masson's trichrome (MTC) staining was performed to further evaluate regenerated bone tissue at the central regions of defect site (Figure 7**)**. After 4 weeks, almost no new bone tissue was formed in the blank group. By contrast, a visible amount of red calcified bone tissue was found in P/A-pDual group. Abundant new collagen fiber bundles, evidently distributed osteocytes and blood vessels were also observed, indicating that bone regeneration was progressing well. After 8 weeks, the amount of newly formed bone increased in all groups. However, only a limited amount of new bone tissue was observed in the blank group, suggesting a low level of bone healing. In P/A-pDual group, thick and organized collagen fibers and a large amount of red-stained bone tissue was observed, indicating the calcification and maturation of new bone. Haversian canals were observed in the lamellar bone. Osteocytes were embedded in lacunae and osteoblasts were lined along the bone surface, demonstrating an active metabolic activity at the regenerated tissue site. In addition, bone marrow was reconstituted around the bridged bone (Supplementary Figure S7), suggesting the later stage of bone remodeling.

To further study the therapeutic effect of the dual-gene delivery scaffold and provide more detailed information for the *in vivo* bone regeneration, immunofluorescence staining was performed to analyze the expression of angiogenic marker (alpha smooth muscle Actin (α-SMA)) and osteogenic markers (Collagen Type I (COL1) and OCN) (Figure 8**).** α-SMA, expressed in the smooth muscle cells of vessels around endothelial cells, was utilized to locate newly formed blood vessels. P/A-pDual group showed the highest positive expression level of α-SMA among all the groups, implying the angiogenic effect of pVEGF delivery. Moreover, it was found that blood vessels formed in P/A-pDual group were small and in round shape with a thick vascular wall, indicating a high maturity. By contrast, blood vessels formed in blank and P/A group tended to show an elliptical shape with a thin vascular wall, indicating a relatively low maturity. The results were in accordance with those obtained from *in vitro* analysis, indicating that the dual-gene delivery scaffold induced a lasting pro-angiogenic effect through controlled release of pVEGF during the bone healing process. For osteogenic markers, P/A-pDual group showed the highest expression levels when compared with the other two groups. OCN serves as a later osteogenic maker regulating bone mineralization. It was observed that OCN protein was abundantly distributed in P/A-pDual implanted defect, while showing much

lower levels in the blank and P/A group. Likewise, blank and P/A groups showed poor COL1 expression, whereas P/A-pDual implanted defect exhibited evidently distributed COL1 in a well-organized and oriented manner, indicating a higher degree of mineralization. These immunofluorescence staining results were in accordance with the μCT and histological analysis, showing that the spatiotemporal delivery of pBMP2 and pVEGF by P/A-pDual significantly promoted angiogenesis and osteogenesis, thus finally led to accelerated bone healing.

Despite the promising findings, there are potential limitations with the present study. Since the ratio of VEGF to BMP2 can affect bone remodeling,[29] how to precisely control the expression of growth factors via well-defined release of incorporated genes in terms of the timeline and amount may still be a challenge and would need further in-depth investigation. In addition, future studies should be directed to explore the mechanism of gene manipulation involving multiple cell types (such as bone marrow stem cells, endothelial cells, osteoclasts and fibroblasts) in the complicated *in vivo* environment to promote clinical translation.

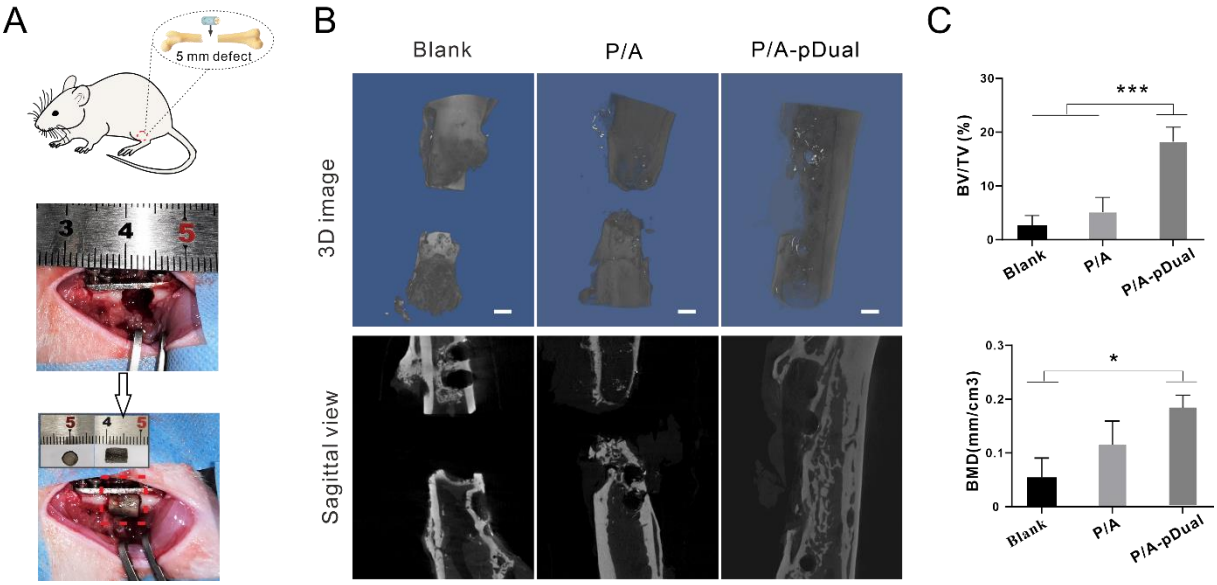

Figure 6. (A) Schematic illustration of the critical-size femoral segmental defect model. The 5-mm defects were treated with none (blank), gene-free scaffold (P/A) and dual gene-activated scaffold (P/A-pDual). Scale bar, 2 mm. (B) Representative μCT images of 3D reconstruction and 2D sagittal-view cross sections of bone repair after 8 weeks of implantation. (C) Quantitative μCT analysis of new bone volume to tissue volume ratios (BV/TV) and BMD. Scale bar = 5 mm. The data were plotted with mean ± standard deviation ($n = 3$). *$p < 0.05$ and ***$p < 0.001$.

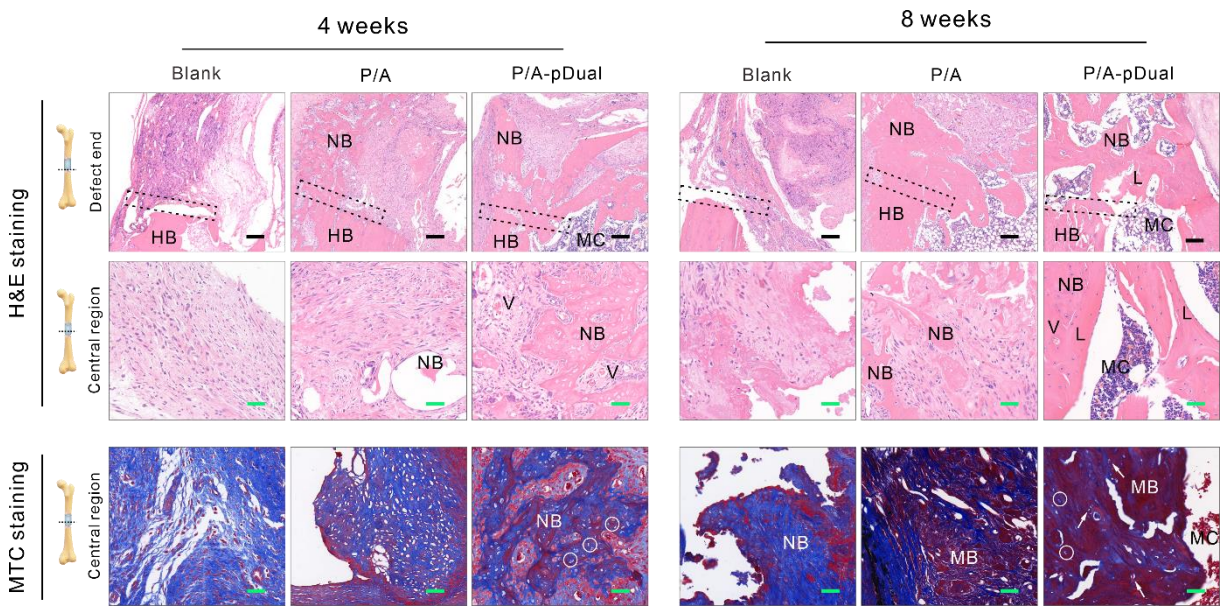

Figure 7. Histological analysis of bone repair after 4 weeks and 8 weeks of implantation by H&E staining and MTC staining. HB: host bone; NB: new bone; MB: mature bone; MC: marrow cavity; L: lamellar; V: vessel; white circles: osteocytes; white arrows: Haversian canal. The dotted square marked the location of bone defect end. The black and green scale bars are 200 μm and 50 μm, respectively.

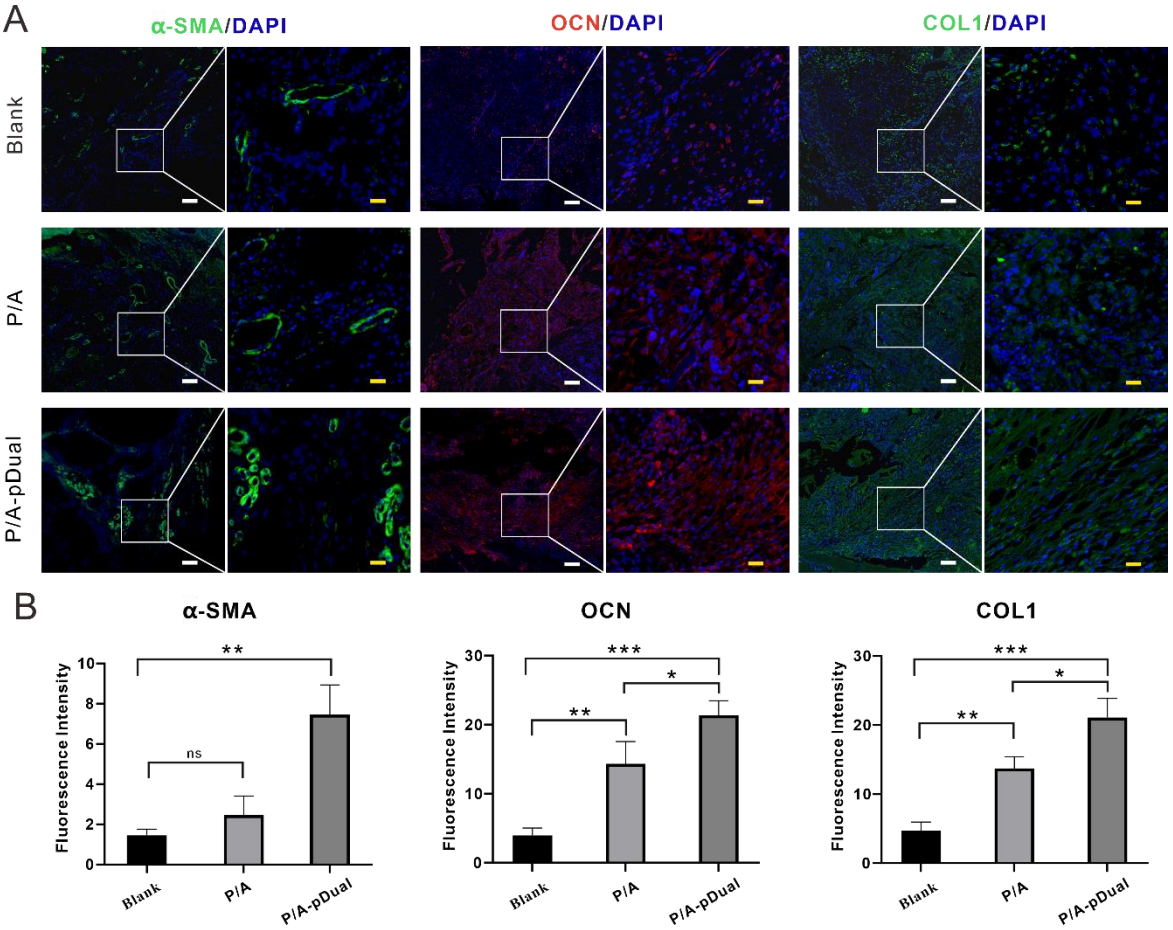

Figure 8. (A) Immunofluorescence staining images of the tissue sections, showing the expression of angiogenic marker α-SMA, and osteogenic markers, OCN and COL1 in the defect area. The nuclei were stained with DAPI. Scale bar, 100 μm. (B) Semi-quantitative analysis of the protein expression using ImageJ. The data were plotted with mean ± standard deviation ($n = 3$). *$p < 0.05$, **$p < 0.01$, and ***$p < 0.001$.

3. Conclusions

The objective of this study was to develop a bioactive fiber-hydrogel composite scaffold to enable spatiotemporally defined gene delivery for vascularized bone regeneration. An efficient non-viral vector, PP@KALA, was developed, which not only promoted proliferation and spreading of pre-osteoblasts, but also induced effective growth factor production via the manipulation of therapeutic genes, pBMP2 and pVEGF. A biomimetic composite scaffold consisting of an alginate hydrogel core and an electrospun PCL fiber sheath was fabricated. pVEGF and pBMP2 were incorporated into the core and sheath respectively and released from the scaffold in a sequential manner. The dual gene-activated core-sheath structured composite scaffold could promote osteogenesis *in vitro*, evidenced by increased calcium deposition and osteogenic gene expression, and enhance bone regeneration in a critical-sized segmental femoral defect model. The present spatiotemporal gene delivery scaffold should be a promising candidate as a bone graft for large bone defect treatment.

Experimental Section

Experimental details are provided in the Supporting Information.

Supporting Information

Supporting Information is available from the Wiley Online Library or from the author.

Acknowledgments

This work was financially supported by the National Key Research and Development Program of China (2016YFB0700803) and Fundamental Research Program of Shenzhen (Grant No. JCYJ20170307110418960), China.

Data availability statement

The data that support the findings of this study are available from the corresponding author upon reasonable request.

Declaration of competing interest

The authors declare no conflict of interest.

Received: ((will be filled in by the editorial staff))
Revised: ((will be filled in by the editorial staff))
Published online: ((will be filled in by the editorial staff))

References

[1] L. Claes, S. Recknagel, A. Ignatius, *Nat. Rev. Rheumatol.* **2012**, 8, 133.

[2] a) S. S. Lee, J. H. Kim, J. Jeong, S. H. L. Kim, R. H. Koh, I. Kim, S. Bae, H. Lee, N. S. Hwang, *Biomaterials* **2020**, 257, 120223; b) L. Wu, Y. Gu, L. Liu, J. Tang, J. Mao, K. Xi, Z. Jiang, Y. Zhou, Y. Xu, L. Deng, L. Chen, W. Cui, *Biomaterials* **2020**, 227, 119555.

[3] T. K. Sampath, S. Vukicevic, *Bone* **2020**, 141, 115602.

[4] T. Niikura, D. J. Hak, A. H. Reddi, *J. Orthop. Res.* **2006**, 24, 1463.

[5] R. Subbiah, M. A. Ruehle, B. S. Klosterhoff, A. S. P. Lin, M. H. Hettiaratchi, N. J. Willett, L. E. Bertassoni, A. J. García, R. E. Guldberg, *Acta Biomater.* **2021**, 127, 180.

[6] a) J. R. Horowitz, A. Rivard, d. Z. R. Van, M. Hariawala, D. D. Sheriff, D. D. Esakof, G. M. Chaudhry, J. F. Symes, J. M. Isner, *Arterloscl. Throm. Vas.* **1997**, 17, 2793; b) C. A. Tannoury, H. S. An, *Spine J.* **2014**, 14, 552.

[7] a) J. Bonadio, E. Smiley, P. Patil, S. Goldstein, *Nat. Med.* **1999**, 5, 753; b) Y. Zha, T. Lin, Y. Li, X. Zhang, Z. Wang, Z. Li, Y. Ye, B. Wang, S. Zhang, J. Wang, *Biomaterials* **2020**, 247, 119985; c) H. Xing, X. Wang, G. Xiao, Z. Zhao, S. Zou, M. Li, J. J. Richardson, B. L. Tardy, L. Xie, S. Komasa, J. Okazaki, Q. Jiang, G. Yang, J. Guo, *Biomaterials* **2020**, 235, 119784; d) D. Lou, Y. Luo, Q. Pang, W.-Q. Tan, L. Ma, *Bioact. Mater.* **2020**, 5, 667.

[8] A. Hadjizadeh, F. Ghasemkhah, N. Ghasemzaie, *Polym. Rev.* **2017**, 57, 505.

[9] a) L. M. Jantz, *Am. J. Phys. Anthropol.* **1999**, 110, 473; b) T. Y. Park, S.-W. Maeng, E. Y. Jeon, K. I. Joo, H. J. Cha, *Biomaterials* **2021**, 272, 120774.

[10] D. Barati, S. R. P. Shariati, S. Moeinzadeh, J. M. Melero-Martin, A. Khademhosseini, E. Jabbari, *J. Control. Release* **2016**, 223, 126.

[11] a) F. Han, X. Jia, D. Dai, X. Yang, J. Zhao, Y. Zhao, Y. Fan, X. Yuan, *Biomaterials* **2013**, 34, 7302; b) W. Zhang, G. Zhou, Y. Gao, Y. Zhou, J. Liu, L. Zhang, A. Long, L. Zhang, P. Tang, *Colloids Surf. B* **2017**, 159, 327.

[12] S. O'Rorke, M. Keeney, A. Pandit, *Prog. Polym. Sci.* **2010**, 35, 441.

[13] a) Y.-H. Lee, H.-C. Wu, C.-W. Yeh, C.-H. Kuan, H.-T. Liao, H.-C. Hsu, J.-C. Tsai, J.-S. Sun, T.-W. Wang, *Acta Biomater.* **2017**, 63, 210; b) T. Gonzalez-Fernandez, S. Rathan, C. Hobbs, P. Pitacco, F. E. Freeman, G. M. Cunniffe, N. J. Dunne, H. O. McCarthy, V. Nicolosi, F. J. O'Brien, D. J. Kelly, *J. Control. Release* **2019**, 301, 13.

[14] S. He, J. Fang, C. Zhong, F. Ren, M. Wang, *Acta Biomater.* **2022**, 140, 149.

[15] a) Y. Chen, Y. Qiu, Q. Wang, D. Li, T. Hussain, H. Ke, Q. Wei, *Chem. Eng. J* **2020**, 399, 125668; b) W. Chen, S. Chen, Y. Morsi, H. El-Hamshary, M. El-Newhy, C. Fan, X. Mo, *ACS Appl. Mater. Inter.* **2016**, 8, 24415.

[16] C. Cheng, S. Li, W. F. Zhao, Q. Wei, S. Q. Nie, S. D. Sun, C. S. Zhao, *J. Membr. Sci.* **2012**, 417, 228.

[17] a) Y. Z. Li, R. Zhao, S. Chao, B. L. Sun, C. Wang, X. Li, *Chem. Eng. J.* **2018**, 344, 277; b) L. Cheng, X. Sun, X. Zhao, L. Wang, J. Yu, G. Pan, B. Li, H. Yang, Y. Zhang, W. Cui, *Biomaterials* **2016**, 83, 169.

[18] T. J. Cho, L. C. Gerstenfeld, T. A. Einhorn, *J. Bone. Miner. Res.* **2002**, 17, 513.

[19] a) P. Mastorakos, A. L. da Silva, J. Chisholm, E. Song, W. K. Choi, M. P. Boyle, M. M. Morales, J. Hanes, J. S. Suk, *P. Natl. Acad. Sci. USA* **2015**, 112, 8720; b) S. E. Est-Witte, A. L. Farris, S. Y. Tzeng, D. L. Hutton, D. H. Gong, K. G. Calabresi, W. L. Grayson, J. J. Green, *Acta Biomater.* **2020**, 113, 279.

[20] a) I. Martins, H. Tomás, F. Lahoz, J. Rodrigues, *Biomacromolecules* **2021**, 22, 2436; b) F. Abedi-Gaballu, G. Dehghan, M. Ghaffari, R. Yekta, S. Abbaspour-Ravasjani, B. Baradaran, J. Ezzati Nazhad Dolatabadi, M. R. Hamblin, *Appl. Mater. Today* **2018**, 12, 177.

[21] a) M. Baghaei, F. S. M. Tekie, M. R. Khoshayand, R. Varshochian, M. Hajiramezanali, M. J. Kachousangi, R. Dinarvand, F. Atyabi, *Mat. Sci. and Eng. C-Mater* **2021**, 118, 111036; b) G.-H. Wang, Y.-Y. Cai, J.-K. Du, L. Li, Q. Li, H.-K. Yang, J.-T. Lin, *Colloid. Surfaces B* **2018**, 162, 326.

[22] O. Boussif, F. Lezoualc'h, M. A. Zanta, M. D. Mergny, D. Scherman, B. Demeneix, J. P. Behr, *Proc. Natl. Acad. Sci.* **1995**, 92, 7297.

[23] a) S. L. Lo, S. Wang, *Biomaterials* **2008**, 29, 2408; b) S. Yamano, J. Dai, S. Hanatani, K. Haku, T. Yamanaka, M. Ishioka, T. Takayama, C. Yuvienco, S. Khapli, A. M. Moursi,

J. K. Montclare, *Biomaterials* **2014**, 35, 1705.

[24] a) S. H. Lee, S. H. Kim, T. G. Park, *Biochem. Bioph. Res. Co.* **2007**, 357, 511; b) T. Gonzalez-Fernandez, B. N. Sathy, C. Hobbs, G. M. Cunniffe, H. O. McCarthy, N. J. Dunne, V. Nicolosi, F. J. O'Brien, D. J. Kelly, *Acta Biomater.* **2017**, 55, 226.

[25] a) L. Parhamifar, A. K. Larsen, A. C. Hunter, T. L. Andresen, S. M. Moghimi, *Soft Matter.* **2010**, 6, 4001; b) A. Hall, U. Lachelt, J. Bartek, E. Wagner, S. M. Moghimi, *Mol. Ther.* **2017**, 25, 1476.

[26] C. P. Ng, T. T. Goodman, I.-K. Park, S. H. Pun, *Biomaterials* **2009**, 30, 951.

[27] a) C. Foerg, U. Ziegler, J. Fernandez-Carneado, E. Giralt, H. P. Merkle, *Pharm. Res.* **2007**, 24, 628; b) F. Heitz, M. C. Morris, G. Divita, *Brit. J. of Pharmacol.* **2009**, 157, 195; c) C. Foerg, U. Ziegler, J. Fernandez-Carneado, E. Giralt, H. P. Merkle, *Pharma. Res-Dordr* **2007**, 24, 628; d) A. Ziegler, *Adv. Drug Deliver. Rev.* **2008**, 60, 580.

[28] A. Hall, *Biochem. Soc. Trans.* **2012**, 40, 1378.

[29] a) Q. Cui, A. S. Dighe, J. N. Irvine, Jr., *Curr. Pharm. Des.* **2013**, 19, 3374; b) A. Hernández, R. Reyes, E. Sánchez, M. Rodríguez-Évora, A. Delgado, C. Évora, *J. Biomed. Mater. Res. A* **2012**, 100A, 2382.

[30] H. Hu, M. J. Hilton, X. Tu, K. Yu, D. M. Ornitz, F. Long, *Development* **2005**, 132, 49.

[31] M. Yamamoto, A. Hokugo, Y. Takahashi, T. Nakano, M. Hiraoka, Y. Tabata, *Biomaterials* **2015**, 56, 18.

Table of Contents

Short summary:

A dual gene-activated biomimetic composite scaffold consisting of an electrospun poly(ε-caprolactone) (PCL) fiber sheath carrying plasmid DNA encoding bone morphogenetic protein 2 (pBMP2) and an alginate hydrogel core carrying plasmid DNA encoding vascular endothelial growth factor (pVEGF) was developed to enable spatiotemporally defined gene delivery for critical-sized segmental bone defect regeneration.

Keyword: Biomimetics

Title: Spatiotemporal Delivery of pBMP2 and pVEGF by a Core-Sheath Structured Fiber-Hydrogel Gene-Activated Matrix Loaded with Peptide-Modified Nanoparticles for Critical-sized Bone Defect Repair

ToC Figure: